Fractal butterflies of Dirac fermions in monolayer and bilayer graphene

Tapash Chakraborty[1], Vadym M. Apalkov[2]

[1]*Department of Physics and Astronomy, University of Manitoba, Winnipeg, R3T 2N2, Canada*
[2]*Department of Physics and Astronomy, Georgia State University, Atlanta, Georgia 30303, USA*
E-mail: Tapash.Chakraborty@umanitoba.ca

Abstract: Bloch electrons in a perpendicular magnetic field exhibit unusual dynamics that has been studied for more than half a century. The single-electron energy spectrum of this system, the Hofstadter butterfly has been the subject of theoretical and experimental investigations for the past two decades. Experimental observation of these unusual spectra in semiconductor nanostructures, however, met with only limited success. The fractal nature of the butterfly spectrum was finally observed in 2013, thanks to the unique electronic properties of graphene. Here, the authors present an overview of the theoretical understanding of Hofstadter butterflies in monolayer and bilayer graphene. First, they briefly discuss the energy spectra in conventional semiconductor systems. The electronic properties of monolayer and bilayer graphene are then presented. Theoretical background on the Moiré pattern in graphene and its application in the magnetoconductance probe that resulted in graphene butterflies are explained. They have also touched upon the important role of electron–electron interaction in the butterfly pattern in graphene. Experimental efforts to investigate this aspect of fractal butterflies have just begun. They conclude by discussing the future prospects of butterfly search, especially for interacting Dirac fermions in graphene.

1 Introduction

The dynamics of an electron in a periodic potential subjected to a perpendicular magnetic field has remained an interesting problem for more than half a century [1–4]. Within the nearest neighbour tight-binding description of the periodic potential the energy spectrum of an electron is described by the Harper equation [2]. Numerical solution of this equation [4] shows that the applied magnetic field splits the Bloch bands into subbands and gaps. The resulting energy spectrum, when plotted as a function of the magnetic flux per lattice cell, reveals a fractal pattern (a self-similar pattern that repeats at every scale) [5] that is known in the literature as Hofstadter's butterfly (because of the pattern resembling the butterflies). This is the first example of the fractal pattern realised in the energy spectra of a quantum system.

A few experimental efforts to detect the butterflies have been reported in the literature. The earlier ones involved artificial lateral superlattices on semiconductor nanostructures [6–11], more precisely the antidot lattice structures with periods of ∼100 nm. The large period (as opposed to those in natural crystals) of the artificial superlattices helps to keep the magnetic field in a reasonable range of values to observe the fractal pattern. Measurements of quantised Hall conductance in such a structure indicated, albeit indirectly, the complex pattern of gaps that were expected in the butterfly spectrum. Hofstadter butterfly patterns were also predicted to occur in other totally unrelated systems, such as, propagation of microwaves through a waveguide with a periodic array of scatterers [12] or more recently, with ultracold atoms in optical lattices [13, 14].

Graphene, a single layer of carbon atoms, arranged in a hexagonal lattice and contains a wealth of unusual electronic properties [15–19] has turned out to be the ideal system in the quest of fractal butterflies. The Dirac fermions in monolayer and bilayer graphene [17, 18] are the most promising objects thus far, where the signature of the recursive pattern of the Hofstadter butterfly has been unambiguously reported [20–22]. Here the periodic lattice with a period of ∼10 nm was created by the Moiré pattern that appears when graphene is placed on a plane of hexagonal boron nitride (h-BN) with a twist [23–25]. Being ultraflat and free of charged impurities, h-BN has been the best substrate for graphene having high-mobility charged fermions [23]. Some theoretical studies have been reported earlier in the literature on the butterfly pattern in monolayer [26] and bilayer graphene [27].

The paper is organised as follows. In Section 2, we briefly describe the background materials leading to the Hofstadter butterfly. The situation in conventional semiconductor systems is presented in Section 3. Section 4 deals with the theories of the butterfly pattern in monolayer graphene, while the theoretical intricacies in bilayer graphene are presented in Section 5. The case of the many-electron system, in particular the influence of the electron–electron interaction on the Hofstadter butterfly pattern is described in Section 6. The concluding remarks are to be found in Section 7.

2 Electrons in a periodic potential and an external magnetic field: Hofstadter butterfly

The dynamics of a two-dimensional (2D) electron in a periodic potential is described by the Hamiltonian [1]

$$\mathcal{H} = \mathcal{H}_0(p_x, p_y) + V(x, y) \qquad (1)$$

which consists of the kinetic energy term $\mathcal{H}_0(p_x, p_y)$ and the periodic potential $V(x, y)$. The most important characteristics of this periodic potential, which determines the dynamics of an electron in a magnetic field is the area S_0 of the unit cell of the periodic structure of $V(x, y)$. For a structure of a simple square lattice type, which is characterised by the lattice constant a_0, the area of a unit cell is $S_0 = a_0^2$. The magnetic field B is introduced in the Hamiltonian (1) via the Peierls substitution, which replaces the momentum (p_x, p_y) by the generalised expression $(p_x - eA_x/c, p_y - eA_y/c)$. Here (A_x, A_y) is the vector potential. We choose the vector potential in the Landau gauge $A = (0, Bx)$. The corresponding Hamiltonian then becomes

$$\mathcal{H} = \mathcal{H}_0(p_x - exB) + V(x, y) \qquad (2)$$

The energy spectra of the Hamiltonian (2) as a function of the magnetic field has the unique fractal structure. Such a structure has a more clear description in the two limiting cases of weak and strong magnetic field. In the case of the weak magnetic field, first, the periodic potential results in the formation of the Bloch bands and then the external magnetic field splits each Bloch band of the periodic potential into minibands of the Landau level (LL) type. In a weak magnetic field, the coupling of different bands can be disregarded. The corresponding Schrödinger equation, which determines the energy spectrum of the system, has a simple form in the tight-binding approximation of the periodic potential, for which the energy dispersion within a single band is [1]

$$E(p_x, p_y) = 2\Delta_0\Big(\cos\left(p_x a_0/\hbar\right) + \cos\left(p_y a_0/\hbar\right)\Big) \qquad (3)$$

where a simple square lattice structure with lattice constant a_0 was assumed. In an external magnetic field, the wave function which is defined at the lattice points (ma_0, na_0), has the form $\Psi(ma, na) = e^{ik_y n}\psi_m$. The corresponding Schrödinger equation reduces to a 1D equation – the so called Harper equation [2]

$$\psi_{m+1} + \psi_{m-1} + 2\cos\Big(2\pi m\tilde{\alpha} - k_y\Big)\psi_m = \varepsilon\psi_m \qquad (4)$$

where $\varepsilon = E/\Delta_0$ and $\tilde{\alpha} = \Phi/\Phi_0$. Here $\Phi = BS_0 = Ba_0^2$ is the magnetic flux through a unit cell and $\Phi_0 = hc/e$ is the magnetic flux quantum. Therefore the dimensionless parameter $\tilde{\alpha}$ is the magnetic flux through a unit cell measured in units of the flux quantum. The energy spectra, determined by the Harper (4), is a periodic function of the parameter $\tilde{\alpha}$ with period 1. Hence it is enough to consider only the values of $\tilde{\alpha}$ within the range $0 < \tilde{\alpha} < 1$. The remarkable property of the Harper (4) is that although the corresponding Hamiltonian is an analytical function of $\tilde{\alpha}$, the energy spectrum (4) is very sensitive to the value of $\tilde{\alpha}$. At rational values of $\tilde{\alpha} = p/q$ the energy spectrum has q bands separated by $q-1$ gaps, where each band is p fold degenerate. As a function of $\tilde{\alpha}$ the energy spectrum (4) has
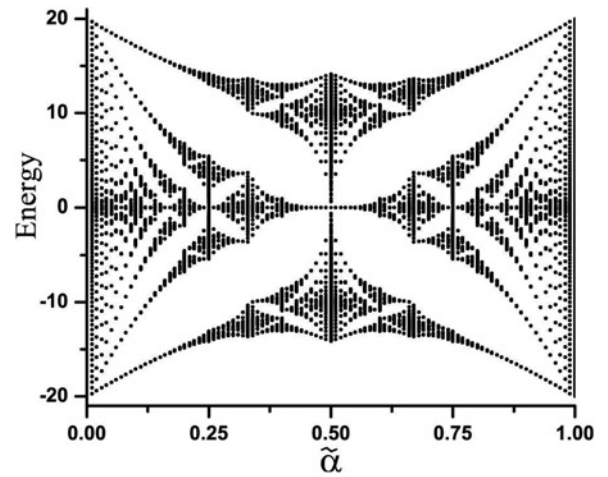
Fig. 1 *Energy spectra (Hofstadter butterfly) of the Harper (4)*
Parameter $\tilde{\alpha}$ is the magnetic flux per unit cell in units of flux quantum

a fractal structure that is known as the Hofstadter butterfly [4]. This structure is shown in Fig. 1. The thermodynamic potential $\Omega_b(T, \mu, \tilde{\alpha})$, corresponding of the system described by the Harper (4), satisfies the following symmetry property [28]

$$\Omega_b(T, \mu, \tilde{\alpha}) = \Omega_b(T, \mu, -\tilde{\alpha}) = \Omega_b(T, \mu, \tilde{\alpha} + 1) \qquad (5)$$

which means that the thermodynamic properties of the system are determined by $0 < \tilde{\alpha} < 1/2$ and $\mu < 0$. Here μ is the chemical potential.

In a strong magnetic field, the energy spectra of the system also show the Hofstadter butterfly fractal structure. Now the periodic potential should be considered as a weak perturbation, which results in a splitting of the corresponding LLs, formed by the strong magnetic field. For a weak periodic potential the inter LL coupling can be disregarded. Then the splitting of a given LL is described by the same Harper-type equation [1]

$$\psi_{m+1} + \psi_{m-1} + 2\cos\Big(2\pi m\alpha - k_y\Big)\psi_m = \varepsilon\psi_m \qquad (6)$$

but now the parameter, which determines the fractal structure of the energy spectrum, is $\alpha = 1/\tilde{\alpha} = \Phi_0/\Phi$–inverse magnetic flux though a unit cell in units of the flux quantum. Therefore for $0 < \alpha < 1$ the energy spectrum has a structure similar to the one shown in Fig. 1. The Hofstadter butterfly energy spectra is realised either as a splitting of the Bloch band by a weak magnetic field or as a splitting of a LL by the weak periodic potential. The thermodynamic properties of these two systems are related by the duality transformation [28]

$$\Omega_L(T, \mu, \alpha) = \alpha\Omega_b(T, \mu, \tilde{\alpha}) \qquad (7)$$

where $\Omega_L(T, \mu, \alpha)$ is the thermodynamic potential within a single LL and weak periodic potential.

For intermediate values of the magnetic field, the mixing of the LL by the periodic potential or the mixing of Bloch bands by the magnetic field becomes strong. This will modify the universality of the butterfly structure and add some system-dependent features. In the following sections, we consider the limits of high and intermediate magnetic fields

for conventional semiconductor systems and the monolayer and bilayer graphene.

3 Conventional semiconductor systems: strong field limit

For strong and intermediate magnetic fields, the periodic potential is considered as a perturbation, which can modify and mix the states of the zero-order Hamiltonian, consisting of the kinetic part only $\mathcal{H}_0(p_x - eA_x/c, p_y - eA_y/c)$. For conventional semiconductor systems, the zero-order Hamiltonian is described by the parabolic dispersion relation, $p^2/2m$. The transverse magnetic field results in Landau quantisation where the LLs are characterised by the Landau level index $n = 0, 1, 2, \ldots$ with energies $E_n = (n + 1/2)\hbar\,\omega_{c,B}$. Here $\omega_{c,B} = eB/mc$ is the cyclotron frequency. The corresponding Landau wave functions $\phi_{n,k}$ have the form

$$\phi_{n,k}(x, y) = \frac{e^{iky}}{\sqrt{L}} \frac{e^{-(x-x_k)^2/2\ell_0^2}}{\sqrt{\pi^{1/2}\ell_0 2^n n!}} H_n(x - x_k) \qquad (8)$$

where L is the length of a sample in the y direction, k is the y component of the electron wave vector, $\ell_0 = \sqrt{c\hbar/eB}$ is the magnetic length, $x_k = k\ell_0^2$ and $H_n(x)$ are the Hermite polynomials.

We consider a system in a periodic external potential that has the form

$$V(x, y) = V_0\Big[\cos(q_x x) + \cos(q_y y)\Big] \qquad (9)$$

where V_0 is the amplitude of the periodic potential, $q_x = q_y = q_0 = 2\pi/a_0$, and a_0 is a period of the external potential $V(x, y)$. The periodic potential mixes the electron states $\phi_{n,k}$ within a single LL, that is, states with the same value of LL index n and different values of k, and also mixes the states of different LLs with different indices n. The strength of the mixing is determined by the matrix elements of the periodic potential $V(x, y)$ between the LL states $\phi_{n,k}$.

The matrix elements of the periodic potential $V(x, y)$ in the basis $\phi_{n,k}(x, y)$ are

$$\langle\phi_{n',k'}|\cos(q_0 y)|\phi_{n,k}\rangle$$
$$= \frac{i^{|n'-n|-(n'-n)}}{2}\Big\{\delta_{k',k+q_0} + (-1)^{n-n'}\delta_{k',k-q_0}\Big\}M_{n',n} \qquad (10)$$
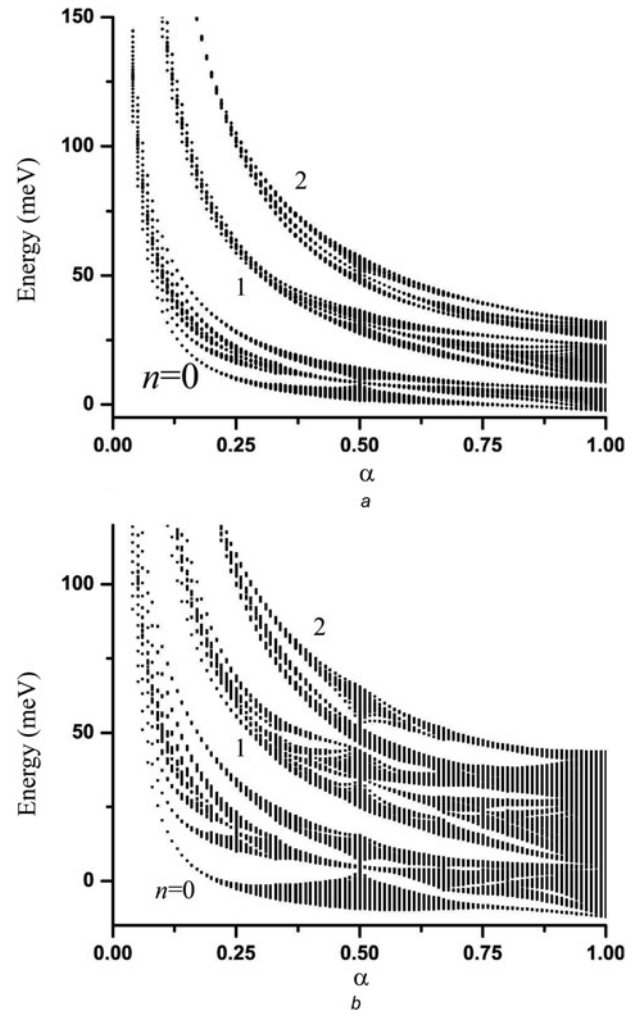
and

$$\langle\phi_{n',k'}|\cos(q_0 x)|\phi_{n,k}\rangle$$
$$= i^{|n'-n|}\frac{\delta_{k',k}}{2}\Big[e^{iq_0 k\ell_0^2} + (-1)^{n-n'}e^{-iq_0 k\ell_0^2}\Big]M_{n',n} \qquad (11)$$

Here

$$M_{n',n} = \left(\frac{m!}{M!}\right)^{1/2} e^{-Q/2} Q^{|n'-n|/2} L_m^{|n'-n|}(Q) \qquad (12)$$

$Q = q_0^2\ell_0^2/2$, $m = \min(n', n)$ and $M = \max(n', n)$.

The matrix elements (10) and (11) determine the mixture of the LL states introduced by the periodic potential. While the

Fig. 2 *Single-electron energy spectra of conventional semiconductor systems with parabolic dispersion relation*

Period of the potential is $a_0 = 20$ nm and its amplitude is
a $V_0 = 10$ meV
b $V_0 = 20$ meV
Energy spectra are shown as a function of the parameter $\alpha = \Phi_0/\Phi$
Numbers indicate the LL index n

component of the potential periodic in the x direction (11) couples only the states with the same value of the wave vector k, the component periodic in the y direction couples the states with the wave vectors separated by q_0. Within a single LL the potential periodic in the x direction modifies the energy of each Landau state. As a result the energy of the Landau state within a given LL becomes a periodic function of $q_0 k\ell_0^2$. Additional coupling of the states separated by q_0, which is determined by (10), results in the formation of the band structure when $q_0^2 l_0^2$ becomes a rational fraction of 2π, which is exactly the condition that the parameter α is rational. It follows from (10) and (11) that for a given LL with an index n the effective amplitude of the periodic potential acquires an additional factor and becomes $\propto V_0 M_{n,n} \propto L_n(q_0^2\ell_0^2/2) = L_n(\pi\alpha)$. These renormalised amplitudes determine the width of the corresponding bands. At values of α where $L_n(\pi\alpha) = 0$, all bands have zero width which correspond to the flatband condition [6, 7].

In general, the expressions for the matrix elements (11) and (10) can be used to find the energy spectra of any finite number of LLs, taking into account the coupling of different LLs introduced by the periodic potential. For a

given value of k within the interval $0 < k < q_0$, a finite set of basis wave functions $\phi_{n,k}$, $\phi_{n,k+q_0}$, $\phi_{n,k+2q_0}$, ..., $\phi_{n,k+N_x q_0}$ is considered. Here $n = 0$, ..., N_L, N_L is the number of LLs, and N_x determines the size of the system in the x direction: $L_x = N_x q_0 \ell_0^2$. The matrix elements (10) and (11) determine the coupling of the states within this truncated basis and finally determines the corresponding Hamiltonian matrix. The diagonalisation of the matrix provides the energy spectrum for a given value of k. The spectra are calculated for a finite number N_y of k points, where N_y determines the size of the system in the y direction: $L_y = 2\pi N_y / q_0$.

Following this procedure, the energy spectra of the conventional system with parabolic dispersion relation were evaluated for $N_L = 2$ LLs. The results are shown in Fig. 2 for the period of the potential $a_0 = 20$ nm. The results clearly show that while for the potential amplitude $V_0 = 10$ meV the mixing of LLs is relatively weak, for a higher amplitude $V_0 = 20$ meV the mixing becomes strong especially for α close to 1, that is, in weak magnetic fields. The butterfly structure is no longer described by the simple Harper equation. In [29], a detailed analysis of the Hofstadter butterfly spectrum was done for strong and intermediate periodic potential strength. The magnetic field splits the Bloch bands and introduces coupling of the states of different Bloch bands.

4 Monolayer graphene

4.1 Square lattice periodic structure

The unique feature of graphene is a relativistic-like low-energy dispersion relation [15, 16], corresponding to the Dirac fermions [17, 18], which results in several unique features in Landau quantisation and in the structure of the LLs. The LLs in graphene have 2-fold valley degeneracy corresponding to two valleys K and K'. The degeneracy cannot be lifted by the periodic potential with typical long periods, $a_0 > 10$ nm. In this case, the Hofstadter butterfly pattern realised in graphene have 2-fold valley degeneracy and it is enough to consider only the states of one valley, for example, valley K. The corresponding Hamiltonian $\mathcal{H}_0$ is written [15, 16] in the matrix form

$$\mathcal{H}_0 = v_F \begin{pmatrix} 0 & \pi_x - i\pi_y \\ \pi_x + i\pi_y & 0 \end{pmatrix} \qquad (13)$$

where $\pi = p + eA/c$, p is the electron momentum and $v_F \simeq 10^6$ m/s is the Fermi velocity.

The LLs in graphene, which are determined by the Hamiltonian (13), are specified by the Landau index $n = 0$, ± 1, ± 2, ..., where the positive and negative values correspond to the conduction and valence band levels, respectively. The energy of the LL with index n is [15, 16]

$$E_n^{(gr)} = s_n \hbar \, \omega_{gr,B} \sqrt{|n|} \qquad (14)$$

where $\omega_{gr,B} = v_F / \ell_0$ is the cyclotron frequency in graphene; $s_n = 1$ for $n > 1$, $s_n = 0$ for $n = 0$ and $s_n = -1$ for $n < 1$.

The eigenfunctions of the Hamiltonian (13), corresponding to the LL with index n, are given by

$$\Psi_{n,k} = C_n \begin{pmatrix} s_n i^{|n|-1} \phi_{|n|-1,k} \\ i^{|n|} \phi_{|n|,k} \end{pmatrix} \qquad (15)$$
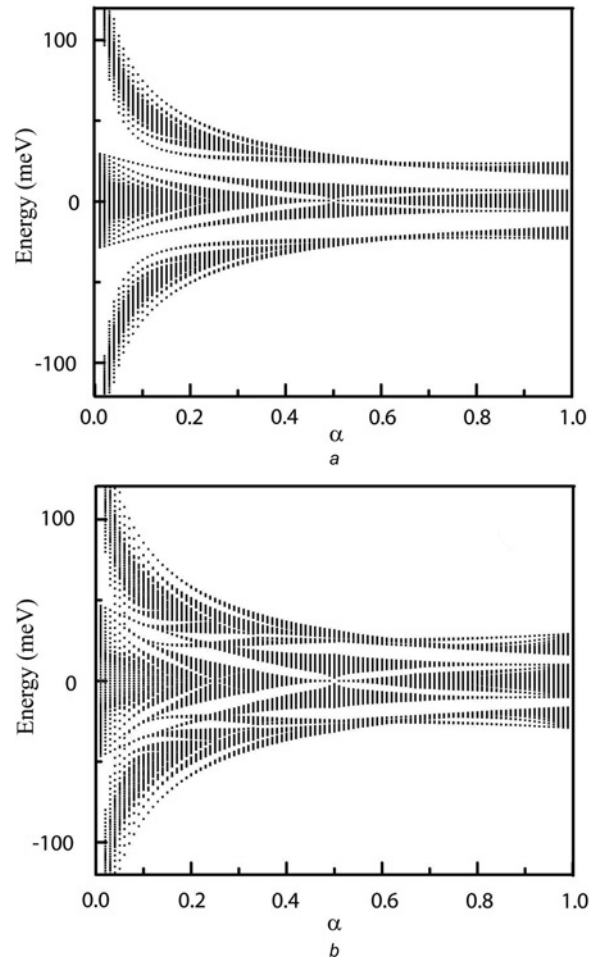
Fig. 3 *Single-electron energy spectra of graphene monolayer in a periodic potential and an external magnetic field*

Period of the potential is $a_0 = 20$ nm and its amplitude is
a $V_0 = 50$ meV
b $V_0 = 100$ meV
Energy spectra are shown as a function of the parameter $\alpha = \Phi_0 / \Phi$

where $C_n = 1$ for $n = 0$ and $C_n = 1/\sqrt{2}$ for $n \neq 0$. Here $\phi_{n,k}$ is the Landau wave function introduced by (8) for an electron with parabolic dispersion relation. The graphene monolayer is then placed in a weak periodic potential $V(x, y)$, which is given by (9). This potential introduces coupling of LLs in graphene. The corresponding matrix elements of the periodic potential are

$$\langle n'k' | \cos(q_0 y) | nk \rangle = \frac{i^{n-n'}}{2} C_n C_{n'} \left\{ \delta_{k',k+q_0} + (-1)^{n-n'} \delta_{k',k-q_0} \right\}$$
$$\times \left[s_n s_{n'} M_{|n'|-1,|n|-1} + M_{|n'|,|n|} \right] \qquad (16)$$

and

$$\langle n'k' | \cos(q_0 x) | nk \rangle$$
$$= \frac{\delta_{k',k}}{2} C_n C_{n'} e^{-iq_0 k \ell_0^2}$$
$$\times \left[1 + (-1)^{n-n'} \right] \left[s_n s_{n'} M_{|n'|-1,|n|-1} + M_{|n'|,|n|} \right] \qquad (17)$$

For a given LL with index n, the periodic potential is

determined by the effective value

$$V_0\big[s_n^2 M_{|n|-1,|n|-1} + M_{|n|,|n|}\big] \propto V_0\big[s_n^2 L_{|n|-1}(\pi\alpha) + L_{|n|}(\pi\alpha)\big] \tag{18}$$

The flatbands in graphene are therefore realised at points where $s_n^2 L_{|n|-1}(\pi\alpha) + L_{|n|}(\pi\alpha)$ is 0. For $n=0$, that is, $s_0=0$, this is exactly the same condition as in conventional systems, but for other LLs the condition of flatbands becomes $L_{|n|-1}(\pi\alpha) + L_{|n|}(\pi\alpha) = 0$.

In Fig. 3, the Hofstadter butterfly energy spectra is shown for a graphene monolayer, taking into account three LLs with $n = -1$, 0 and 1. The main difference between the conventional systems and graphene is the broadening of the energy structure within a single LL. For conventional system (Fig. 2), the width of the energy spectra for the $n = 1$ LL is small for small values of α and large for large α. In graphene, the behaviour is different: the broadening of the $n = 1$ LL is large for small values of α and small for intermediate and large values of α. Another specific feature of the energy spectra of graphene is that the mixing of the LLs, introduced by the periodic potential, is visible for much large values of the amplitude of the potential, $V_0 \simeq 100$ meV compared to $V_0 \simeq 20$ meV in conventional systems (Fig. 2b).

4.2 Moiré structure

With the system of graphene one has the unique possibility to generate in the Hamiltonian a periodical perturbation (periodic potential) based on the intrinsic structure of graphene-based systems. Such a periodic structure is based on the Moiré pattern which appears between two similar regular structures overlaid at an angle. In graphene, the Moiré pattern is realised in (i) twisted bilayer graphene [30–39] which consists of two monolayers with the relative small rotation angle between the layers; and (ii) graphene monolayer on hexagonal boron nitride substrate with rotational misalignment between the graphene monolayer and the h-BN [20–23, 40, 41]. Realisation of the Moiré pattern in two hexagonal lattices (layers) is shown in Fig. 4. That pattern introduces a large-scale periodicity in the Hamiltonian of the systems, which, in a magnetic field, results in the Hofstadter butterfly spectra.

For twisted bilayer graphene, the periodical modulation of the Hamiltonian is introduced through the interlayer hopping coupling, which capture the periodic structure of the Moiré pattern. The interlayer coupling matrix is [38]

$$T(\boldsymbol{r}) = w \sum_j e^{-i\boldsymbol{q}_j \boldsymbol{r}} \boldsymbol{T}_j \tag{19}$$

where $j = 1, 2, 3$ and matrices $\boldsymbol{T}_j$ have the form

$$T_1 = \begin{pmatrix} 1 & 1 \\ 1 & 1 \end{pmatrix}, \quad T_2 = \begin{pmatrix} e^{-i\psi} & 1 \\ e^{i\psi} & e^{-i\psi} \end{pmatrix}, \quad T_3 = \begin{pmatrix} e^{i\psi} & 1 \\ e^{-i\psi} & e^{i\psi} \end{pmatrix} \tag{20}$$

Here $\psi = 2\pi/3$, $\boldsymbol{q}_1 = k_D\theta(0, -1)$, $\boldsymbol{q}_2 = k_D\theta(\sqrt{3}/2, 1/2)$, $\boldsymbol{q}_3 = k_D\theta(-\sqrt{3}/2, 1/2)$, θ is the twist angle, k_D is the Dirac momentum and w is the hopping energy. The interlayer coupling has a matrix form, where the two components of the matrix correspond to two layers of graphene bilayer.
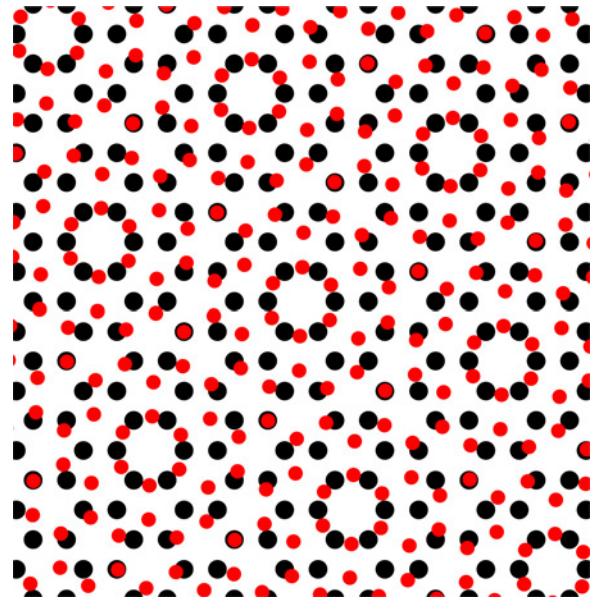

Fig. 4 *Moiré pattern in two hexagonal lattices with rotational misalignment*

Two lattices, which correspond to two layers are shown by red and black dots, respectively

The Moiré periodicity in the matrix $\boldsymbol{T}(\boldsymbol{r})$ results in the formation of the Hofstadter butterfly pattern, which was studied in [38] as a splitting of the Landau levels because of the weak periodical modulation of $\boldsymbol{T}(\boldsymbol{r})$. Since the area of the Moiré units cell is $\propto 1/\theta^2$, to observe the Hofstadter butterfly pattern for experimentally realised magnetic fields the twist angle should be small, $\theta \lesssim 5^0$.

Just as for the twisted bilayer graphene, the periodical perturbation in the Hamiltonian of monolayer graphene placed on a h-BN substrate is introduced through the periodical modulation of the interlayer coupling. The difference from the bilayer graphene case is that there is a small $\simeq 1.8\%$ lattice mismatch between the graphene and the BN. As a result, the interlayer coupling is determined by both the lattice mismatch and rotational misalignment by an angle θ. Then the corresponding superlattice period a_0 depends both on the twist angle and the lattice mismatch. Even in the case of perfect alignment, that is, for the zero twist angle, the superlattice period is $a_0 \simeq 13$ nm. This value introduces upper limits on the superlattice period. This is different from twisted graphene bilayer, for which there is no superlattice for perfect alignment of the layers and there is no constraint on the values of a_0. Another specific feature of graphene monolayer on the h-BN substrate is an asymmetry term in the effective Hamiltonian of graphene, which is because of different couplings of the B and N atoms to the graphene layer.

The periodic perturbation of the graphene Hamiltonian on the h-BN substrate, that is, the graphene superlattice, results in the formation of multiple Moiré minibands and generation of secondary Dirac points [40–42] near the edges of the superlattice Brillouin zone. These points are characterised by the wave vector $G = 4\pi/\sqrt{3}a_0$. The energy corresponding to this vector is $E_G = \hbar v_F G/2$. To observe these secondary Dirac points the graphene should be doped upto energy E_G. Since the period of the Moiré superlattice is determined by the twist angle, the doping requirement introduces a constraint on the values of the twist angle, which should be less than $1°$ [22]. The
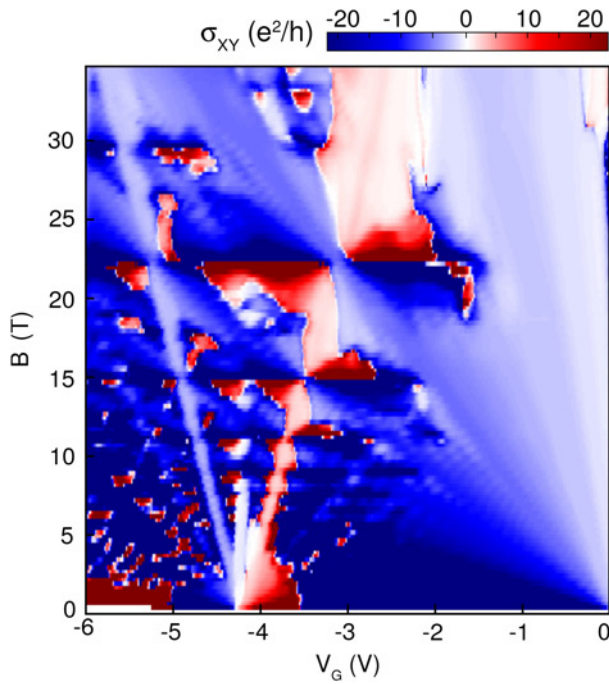
Fig. 5 *Experimental results for the Hall conductance probe of minigap opening within a Landau level in graphene, depicting the self-similarity pattern*

(Courtesy of P. Kim and C. Dean)

formation of the fractal Hofstadter butterfly pattern in graphene on the h-BN substrate was studied theoretically in [42] and was later observed experimentally in [20–22]. This butterfly pattern was realised as splitting of the Moiré minibands (secondary Dirac cones) by a magnetic field. An example of the experimental results from the magnetoconductance probe of the minigap opening in graphene is shown in Fig. 5, where the fractal pattern is clearly visible.

5 Bilayer graphene

Bilayer graphene consists of two coupled monolayers. This coupling opens a gap in the low energy dispersion relation and, in a magnetic field, modifies the LL structure. We consider the bilayer graphene with Bernal stacking. A single-particle Hamiltonian (kinetic energy part) of this system in a magnetic field is [43, 44]

$$
\mathcal{H}_\xi^{(bi)} = \xi \begin{pmatrix}
\dfrac{U}{2} & v_F \pi_- & 0 & 0 \\
v_F \pi_+ & \dfrac{U}{2} & \xi \gamma_1 & 0 \\
0 & \xi \gamma_1 & -\dfrac{U}{2} & v_F \pi_- \\
0 & 0 & v_F \pi_+ & -\dfrac{U}{2}
\end{pmatrix} \quad (21)
$$

where $\xi = \pm 1$ corresponds to two valley (K and K'), U is the inter-layer bias voltage which can be varied for a given system, and $\gamma_1 \simeq 0.4$ eV is the inter-layer coupling. The eigenfunctions of the Hamiltonian (21) can be expressed in

term of the Landau functions $\phi_{n,k}$ (8)

$$
\Psi_{n,k}^{(bi)} = \begin{pmatrix}
\xi C_1 \phi_{|n|-1,k} \\
i C_2 \phi_{|n|,k} \\
i C_3 \phi_{|n|k} \\
\xi C_4 \phi_{|n|+1,k}
\end{pmatrix} \quad (22)
$$

where the coefficients, C_1, C_2, C_3 and C_4, can be found from the following system of equations

$$
\varepsilon C_1 = \xi u C_1 - \sqrt{n} C_2 \quad (23)
$$

$$
\varepsilon C_2 = \xi u C_2 - \sqrt{n} C_1 + \tilde{\gamma}_1 C_3 \quad (24)
$$

$$
\varepsilon C_3 = -\xi u C_3 + \sqrt{n+1} C_4 + \tilde{\gamma}_1 C_2 \quad (25)
$$

$$
\varepsilon C_4 = -\xi u C_4 + \sqrt{n+1} C_3 \quad (26)
$$

Here all energies are expressed in units of $\varepsilon_B = \hbar v_F / \ell_0$, ε is the energy of the LL, $u = U/(2\varepsilon_B)$, and $\tilde{\gamma}_1 = \gamma_1 / \varepsilon_B$. The energy spectra of the LLs can be found from [45]

$$
\left[(\varepsilon + \xi u)^2 - 2n \right]\left[(\varepsilon - \xi u)^2 - 2(n+1) \right] = \tilde{\gamma}_1^2 \left[\varepsilon^2 - u^2 \right] \quad (27)
$$

For each value of $n \geq 0$ there are four solutions of the eigenvalue (27), corresponding to four Landau levels in a bilayer graphene for a given valley, $\xi = \pm 1$. For zero bias voltage, $U = 0$ these four Landau levels are

$$
\varepsilon = \pm \sqrt{2n + 1 + \frac{\tilde{\gamma}_1^2}{2} \pm \frac{1}{2}\sqrt{(2 + \tilde{\gamma}_1^2)^2 + 8n\tilde{\gamma}_1^2}} \quad (28)
$$

In this case, each Landau level has 2-fold valley degeneracy which is lifted at finite bias voltage U.

For $n = 0$, there are two special LLs of bilayer graphene. One LL has the energy $\varepsilon = -\xi u$ and the wave function of this LL consists of $\phi_{0,k}$ functions only

$$
\Psi_{0_1,k}^{(bi)} = \begin{pmatrix}
\phi_{0,k} \\
0 \\
0 \\
0
\end{pmatrix} \quad (29)
$$

This LL of bilayer graphene has exactly the same properties as for the 0th conventional, non-relativistic Landau level. For zero bias voltage U, this level has zero energy.

For small values of U there is another solution of (27) with $n = 0$, which has almost zero energy, $\varepsilon \simeq 0$. The corresponding LL has the wavefunction

$$
\Psi_{0_2,k}^{(bi)} = \frac{1}{\sqrt{\gamma_1^2 + 2\varepsilon_B^2}} \begin{pmatrix}
\gamma_1 \phi_{1,k} \\
0 \\
\sqrt{2}\varepsilon_B \phi_{0,k} \\
0
\end{pmatrix} \quad (30)
$$

The wave function of this LL is the mixture of the $n = 0$ and $n = 1$ conventional (non-relativistic) Landau functions $\phi_{0,k}$ and $\phi_{1,k}$. This mixing depends on the magnitude of the magnetic field. In a small magnetic field, $\varepsilon_B \ll \gamma_1$, the wavefunction is $(\psi_{1,m}, 0, 0, 0)^T$ and the LL is identical to the $n = 1$ non-relativistic LL. In a large magnetic field $\varepsilon_B \gg \gamma_1$, the LL wavefunction is $(0, 0, \psi_{0,m}, 0)^T$ and the bilayer LL has the same properties as the $n = 0$ non-relativistic LL.

Following the same procedure as for the conventional systems and the graphene monolayer, we can find the matrix elements of the periodic potential in the basis of LL wave function of bilayer graphene

$$\langle n'k' | \cos(q_0 y)|nk\rangle$$
$$= \frac{i^{n-n'}}{2} C_n C_{n'} \left\{ \delta_{k',k+q_0} + (-1)^{n-n'} \delta_{k',k-q_0} \right\}$$
$$\times \left[C_{n,1} C_{n',1} M_{|n'|-1,|n|-1} + C_{n,4} C_{n',4} M_{|n'|+1,|n|+1} \right.$$
$$\left. + (C_{n,2} C_{n',2} + C_{n,3} C_{n',3}) M_{|n'|,|n|} \right]$$

(31)

and

$$\langle n'k' | \cos(q_0 x)|nk\rangle$$
$$= \frac{\delta_{k',k}}{2} C_n C_{n'} e^{-iq_0 k \ell_0^2} \left[1 + (-1)^{n-n'} \right]$$
$$\times \left[C_{n,1} C_{n',1} M_{|n'|-1,|n|-1} + C_{n,4} C_{n',4} M_{|n'|+1,|n|+1} \right.$$
$$\left. + (C_{n,2} C_{n',2} + C_{n,3} C_{n',3}) M_{|n'|,|n|} \right].$$

(32)

With the known matrix elements of the periodic potential, we can find the energy spectra of bilayer graphene in a magnetic field and weak (or intermediate) periodic potential, taking into account many LLs. The results are shown in Fig. 6. For zero bias voltage (Fig. 6a), similar to graphene, the inter-Landau level coupling becomes important only for large amplitudes of the periodic potential, $V_0 > 100$ meV. This is true except for two degenerate LLs of type (29) and (30), for which the inter-level coupling becomes strong even for small amplitudes V_0 because of the degeneracy of the levels. In this case, the structure of the energy spectrum near zero energy becomes complicated because of the mixture of two degenerate butterfly structures. These two butterfly structures are not identical because of different types of wave functions of the two LLs and correspondingly different effective periodic potentials. For one LL, the effective periodic potential is $V_0 L_0(\pi \alpha)$, while for the other LL, the wave function of which is given by (30), the effective strength of the potential is

$$\frac{V_0}{\gamma_1^2 + 2\varepsilon_B^2} \left(\gamma_1^2 L_1(\pi \alpha) + 2\varepsilon_B^2 L_0(\gamma_1^2 L_0(\pi \alpha)) \right)$$

(33)

At a finite bias voltage (Figs. 6b and c) the degeneracy of two low energy LLs is lifted and we can observe two distinctively separated butterfly structures for large values of α. For small α (large magnetic field), there is a large overlap of the two butterfly structures and a strong inter-level mixture is expected. In one of the initially degenerate LLs the flatband condition is satisfied for $\alpha \simeq 0.35$ (Fig. 6c). The Hofstadter butterfly in bilayer graphene has been studied in [27], where general configuration of the bilayer graphene, for example, continuous displacement between the layers, was introduced.

6 Interaction effects

6.1 Hartree approximation

Theoretical analysis of the Hofstadter butterfly problem was mainly restricted to non-interacting electron systems. There
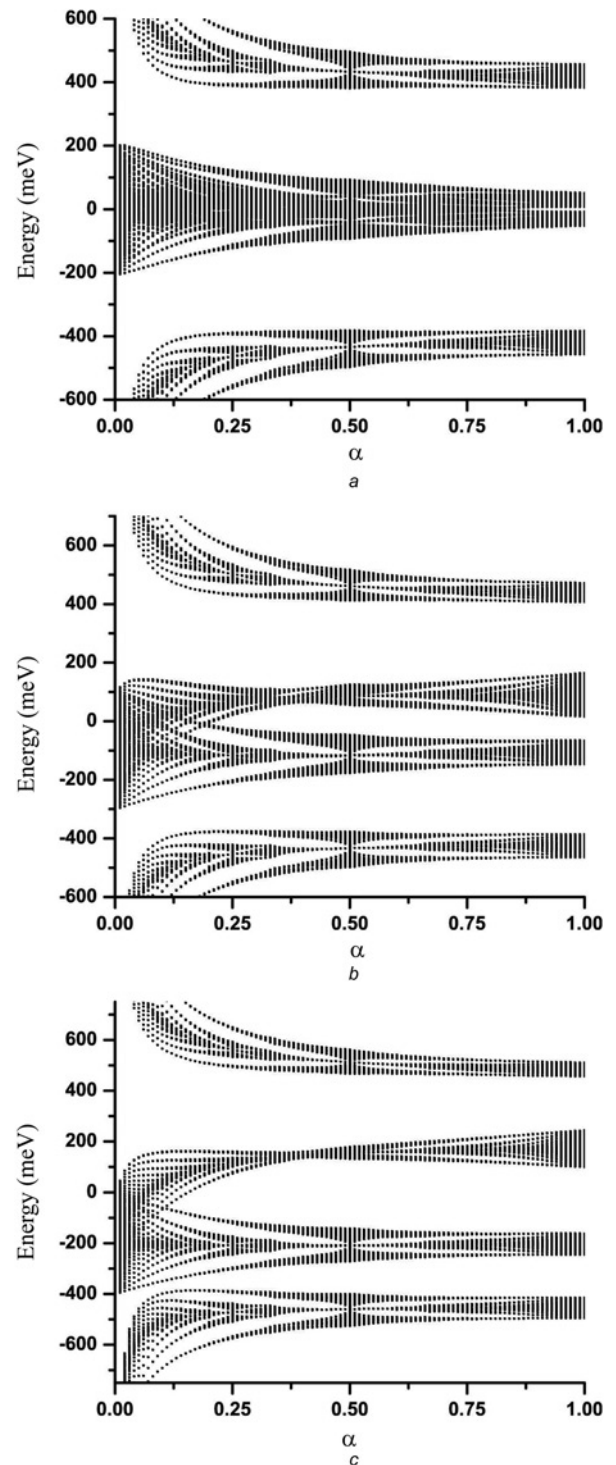
Fig. 6 *Single-electron energy spectra of bilayer graphene in a periodic potential and an external magnetic field*

Period of the potential is $a_0 = 20$ nm and its amplitude is $V_0 = 100$ meV
Bias voltage is
a $U = 0$
b $U = 200$ meV
c $U = 400$ meV
Energy spectra are shown as a function of the parameter $\alpha = \Phi_0/\Phi$

were only a few papers that reported on the effects of electron–electron interactions on the fractal energy spectra [46–51]. The problem with the inclusion of the electron–electron interaction into the system is related to the requirement that the system should have a large size to capture the fractal nature of the spectrum. The Hartree or

mean-field approaches have been used to estimate the effect of interactions on the electron energy spectrum.

In the Hartree approach, the problem is reduced to the single-electron problem in a periodic potential and the Hartree potential, produced by the inter-electron interaction with average electron density. The Hamiltonian of the system with the Hartree interaction is

$$\mathcal{H} = \mathcal{H}_0(p_x, p_y) + V(x, y) + V_H(x, y) \qquad (34)$$

where $V_H(x, y)$ is the Hartree potential, which can be expressed as

$$V_H(x, y) = \int dx_1 dy_1 \frac{e^2}{\kappa |\mathbf{r} - \mathbf{r}_1|} n(\mathbf{r}_1) \qquad (35)$$

Here κ is the background dielectric constant and

$$n(\mathbf{r}) = \sum_i' |\Psi_i(x, y)|^2 \qquad (36)$$

where the prime means that the sum goes over all occupied electron states. The number of occupied states is determined by the chemical potential of the system, μ, that is, only the states with energy E_i less than the chemical potential, $E_i < \mu$, are occupied. The wave functions $\Psi_i(x, y)$ are single-particle wave functions of the Hamiltonian (34).

The finite size system (34)–(36) can be solved numerically following the self-consistent procedure. The final solution is the energy spectrum of the electron system with the Hartree interaction. It is convenient to express the Hartree potential in the reciprocal space. The electron density should have the same spatial symmetry as the periodic potential. Then the Fourier transform of the electron density

$$\tilde{n}(\mathbf{G}) = \frac{1}{A_0} \int d\mathbf{r} n(\mathbf{r}) e^{-i\mathbf{r}\mathbf{G}} \qquad (37)$$

is non-zero only at points of reciprocal lattice, that is, at points $\mathbf{G} = \mathbf{G}_{n_x,n_y} = (2\pi/a_0)(n_x, n_y)$, where n_x and n_y are integers. Here A_0 in (37) is the area of the sample. Then the Fourier transform of the Hartree potential is also non-zero only at points of the reciprocal lattice and is given by

$$V(\mathbf{G}) = \frac{2\pi e^2}{\kappa |\mathbf{G}|} \tilde{n}(\mathbf{G}) \quad \text{for} \quad \mathbf{G} \neq 0 \qquad (38)$$

and $V(\mathbf{G} = 0) = 0$. In [46–48], this approach was used to study the interaction effects on Hofstadter butterfly in conventional systems, where strong oscillations of the LL bandwidth with chemical potential, that is, filling of the LL, were reported.

Following the procedure outlined above, the interaction effects on the band structure of the Hofstadter butterfly in graphene were studied in [51]. The graphene LLs with indices $n = 0$, $n = \pm 1$ and $n = \pm 2$ were considered and the gap structure for $\alpha = 1/2$ and $\alpha = 1/3$ with interaction and without interaction were analysed. Periodic boundary conditions were applied and the size of the system was $50a_0 \times 50a_0$. For $\alpha = 1/2$, the system is expected to have two bands separated by a gap. For non-interacting system the gap is zero at all LLs. Finite electron–electron interactions open gaps for $\alpha = 1/2$, where the magnitude of the gap depends both on the period a_0 of the periodic potential and its magnitude V_0. In Fig. 7, [51] this dependence is shown
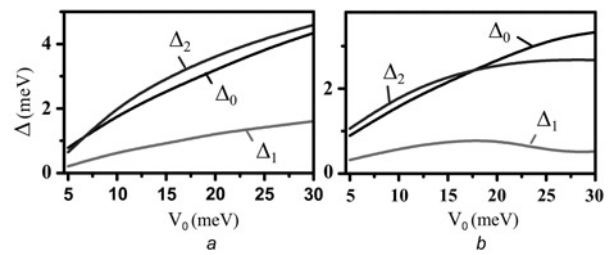
Fig. 7 *Band gaps in the $n = 0$, $n = 1$ and $n = 2$ LLs against the amplitude of the periodic potential, V_0, for interacting systems with half filling of the $n = 0$ Landau level*

Band gap Δ_n at LL with index n is defined as the gap between the corresponding bands of Dirac fermions in a magnetic field corresponding to $\alpha = 1/2$
Period of the potential is
a $a_0 = 20$ nm
b $a_0 = 40$ nm

for the case when half of the $n = 0$ LL is occupied, that is, the chemical potential is zero. Strong non-monotonic dependence of the gaps on the LL index is clearly visible in Fig. 7, and as a function of the LL index the gap has a minimum for $n = 1$.

The case of $\alpha = 1/3$ has been also studied in [51] (Fig. 8). In this case, even without the interaction, the system has three bands and correspondingly two non-zero gaps in each LL. For a non-interacting system the two gaps $i = 1, 2$ in the LL with index n are labelled as $\Delta_{n,i}^{(0)}$. Owing to the symmetry the two gaps in the $n = 0$ LL are the same, $\Delta_{01}^{(0)} = \Delta_{02}^{(0)}$. In higher LLs ($n = 1$ and 2), the two gaps are different because of the LL mixing introduced by the periodic potential. Then the gaps in the same LL are different, for example, $\Delta_{11}^{(0)} \neq \Delta_{12}^{(0)}$. Interaction modifies the gaps with the general
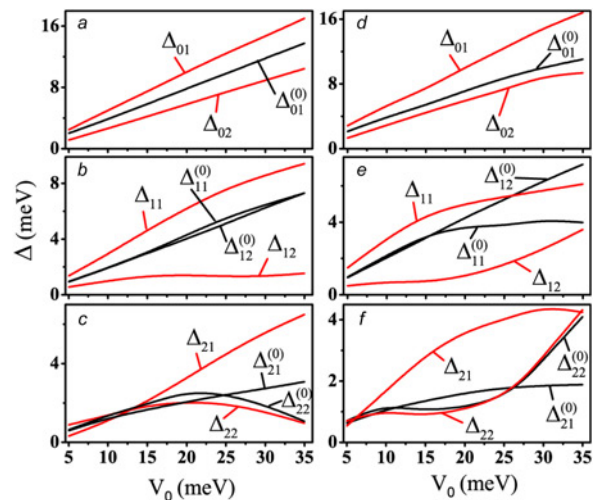
Fig. 8 *Band gaps against V_0 for*

a, d $n = 0$
*b, e* $n = 1$
c, f $n = 2$ LLs
Band gaps are defined as the gaps between the corresponding bands of Dirac fermions in a magnetic field for $\alpha = 1/3$
Black lines correspond to the case of the non-intercting system, while the red lines correspond to the Dirac fermions with Hartree interaction and half filling of the $n = 0$ Landau level
Gaps are labelled as $\Delta_{ni}^{(0)}$ (non-interacting system) and Δ_{ni} (interacting system), where n is the LL index and $i = 1$ and 2 corresponds to the low-energy and high energy gaps, respectively
Period of the periodic potential is $a_0 = 20$ nm (a, b and c) and $a_0 = 40$ nm (d, e and f)
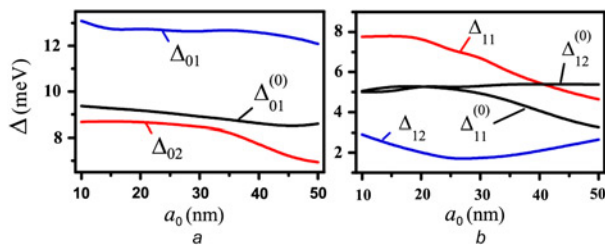
Fig. 9 *Band gaps in*

a n = 0

b n = 1 LLs against the period a_0 of the periodic potential for non-interacting system and the system with interaction and half filling of the $n = 0$ Landau level for $\alpha = 1/3$

Amplitude of the potential is $V_0 = 25$ meV

tendency that the lower energy gap is enhanced and the higher one is suppressed. For $n = 0$ the two gaps are no longer equal, $\Delta_{01} \neq \Delta_{02}$. As a function of the amplitude of the periodic potential the gaps have a non-monotonic dependence with local minimum (or maximum) at finite values of V_0. The higher energy gap for $n = 1$, Δ_{12}, is strongly suppressed by the electron–electron interactions (Fig. 8).

The enhancement or suppression of the gaps by the electron–electron interactions depend not only on the amplitude of the periodic potential but also on the period of the potential. This dependence is shown in Fig. 9 for $\alpha = 1/3$ and amplitude of the potential $V_0 = 25$ meV. The results are shown for the $n = 0$ and $n = 1$ LLs only. The gaps, both for the system with interactions and without interactions, have weak dependence on a_0 for small values of the period, $a_0 \lesssim 25$ nm. For larger values of a_0 there is a strong suppression of the low energy gap, Δ_{11}, in the $n = 1$ LL and higher energy gap, Δ_{02}, in the $n = 0$ LL. In general, the gaps have monotonic dependence on a_0, except the higher energy gap, Δ_{12}, in the $n = 1$ LL, which has a minimum at $a_0 \simeq 25$ nm.

6.2 Correlation effects: extreme quantum limit

In the extreme quantum limit, that is, in a strong magnetic field and extremely low temperatures, electrons display the celebrated fractional quantum Hall effect (FQHE), which is a unique manifestation of the collective modes of the many-electron system. The effect is driven entirely by the electron correlations resulting in the so-called incompressible states [52–55]. It should be pointed out that the properties of incompressible states of Dirac fermions have been established theoretically for monolayer graphene [56] and bilayer graphene [57, 58] and the importance of interactions in the extreme limit are well known [17, 18, 59–63]. There are also experimental evidence of the FQHE states in graphene [15, 64–67]. The precise role of FQHE in the fractal butterfly spectrum has remained unanswered, however. Interestingly, in a recent experiment [68], the butterfly states in the integer quantum Hall regime [69] have been already explored. Understanding the effects of electron correlations on the Hofstadter butterfly is therefore a pressing issue. In [70], the authors have recently developed the magnetic translation algebra [71, 72] of the FQHE states, in particular for the primary filling factor $\nu = 1/3$ for Hofstadter butterflies in the graphene [73, 74]. They considered a system of electrons in a periodic rectangular geometry that was very useful earlier in studying the properties of the FQHE in the absence of a

periodic potential [75–82]. The work in [70] has unveiled a profound effect of the FQHE states on the butterfly spectrum resulting in a transition from the incompressible FQHE gap to the gap because of the periodic potential alone, as a function of the periodic potential strength. There are also crossing of the ground state and low-lying excited states depending on the number of flux quanta per unit cells, that are absent when the periodic potential is turned off.

The magnetic translation analysis was employed to study the effect of a periodic potential on the FQHE in graphene for the primary filling factor $\nu = 1/3$. For $\alpha = 1/2$ and $\alpha = 1/3$, increasing the periodic potential strength V_0 resulted in a closure of the FQHE gap and the appearance of gaps because of the periodic potential [70]. It was also found that for $\alpha = 1/2$ this results in a change of the ground state and consequently in the change of the ground state momentum. For $\alpha = 1/3$, despite the observation of the crossing between the low-lying energy levels, the ground state does not change with an increase of V_0 and is always characterised by the zero momentum. The difference between these two α s is a result of the origin of the gaps in the energy levels. For $\alpha = 1/2$ the emergent gaps are because of the electron–electron interaction only, whereas for $\alpha = 1/3$ these are both because of the non-interacting Hofstadter butterfly pattern and the electron–electron interaction.

7 Concluding remarks

It has been a while since the beautiful theoretical idea of the Hofstadter butterfly which encompasses the fractal geometry and electron dynamics in a magnetic field and periodic potentials was proposed. The advent of graphene has facilitated the experimental observation of fractal butterflies in real physical systems. The remarkable electronic properties of graphene, briefly describe here, helped in achieving this feat when the experimentalists made tremendous progress in creating the Moiré pattern in graphene by finding the appropriate substrate. Discovery of the fractal butterfly in graphene has opened up new directions of research, both in materials science, and in fundamental studies of 2D electrons. The inherent complexity of the butterfly spectrum is yet to be fully explored, however. Future experiments will undoubtedly be at the limit of strong electron correlations [68], which depend crucially on the superior quality of graphene superlattices, thereby opening up the fertile field of many-body effects on Dirac materials for future explorations.

8 Acknowledgments

9 References

1 Rössler, U., Shurke, M.: 'Bloch electrons in a magnetic field: Hofstadter's butterfly', in Kramer, B. (Ed.): 'Advances in solid state physics' (Springer, 2000), vol. 40, pp. 35–50

2 Harper, P.G.: 'Single band motion of conduction electrons in a uniform magnetic field', *Proc. Phys. Soc. A*, 1955, **68**, (10), pp. 874–879

3 Langbein, D.: 'The tight-binding and the nearly-free-electron approach to lattice electrons in external magnetic fields', *Phys. Rev.*, 1969, **180**, (3), pp. 633–648

4 Hofstadter, D.: 'Energy levels and wave functions of Bloch electrons in rational and irrational magnetic fields', *Phys. Rev. B*, 1976, **14**, (6), pp. 2239–2249

5 Mandelbrot, B.B.: 'The fractal geometry of nature' (W.H. Freeman and Company, 1982)

6 Geisler, M.C., Smet, J.H., Umansky, V., *et al.*: 'Detection of a Landau band-coupling-induced rearrangement of the Hofstadter butterfly', *Phys. Rev. Lett.*, 2004, **92**, (25), p. 256801

7 Geisler, M.C., Smet, J.H., Umansky, V., *et al.*: 'Detection of Landau band coupling induced rearrangement of the Hofstadter butterfly', *Phys. E*, 2004, **25**, (2), pp. 227–232

8 Albrecht, C., Smet, J.H., von Klitzing, K., *et al.*: 'Evidence of Hofstadter's fractal energy spectrum in the quantized Hall conductance', *Phys. Rev. Lett.*, 2001, **86**, (1), pp. 147–150

9 Albrecht, C., Smet, J.H., von Klitzing, K., *et al.*: 'Evidence of Hofstadter's fractal energy spectrum in the quantized Hall conductance', *Phys. E*, 2003, **20**, (1), pp. 143–148

10 Schlösser, T., Ensslin, K., Kotthaus, J.P., *et al.*: 'Internal structure of a Landau band induced by a lateral superlattice: a glimpse of Hofstadter's butterfly', *Europhys. Lett.*, 1996, **33**, (9), pp. 683–688

11 Schlösser, T., Ensslin, K., Kotthaus, J.P., *et al.*: 'Landau subbands generated by a lateral electrostatic superlattice-chasing the Hofstadter butterfly', *Semicond. Sci. Technol.*, 1996, **11**, (11S), pp. 1582–1585

12 Kuhl, U., Stöckmann, H.-J.: 'Microwave realization of the Hofstadter butterfly', *Phys. Rev. Lett.*, 1998, **80**, (15), pp. 3232–3235

13 Aidelsburger, M., Atala, M., Lohse, M., *et al.*: 'Realisation of the Hofstadter Hamiltonian with ultracold atoms in optical lattices', *Phys. Rev. Lett.*, 2013, **111**, (18), p. 185301

14 Miyake, H., Siviloglu, G.A., Kennedy, C.J., *et al.*: 'Realising the Harper Hamiltonian with laser-assisted tunneling in optical lattices', *Phys. Rev. Lett.*, 2013, **111**, (18), p. 185302

15 Aoki, H., Dresselhaus, M.S. (Eds.): 'Physics of Graphene' (Springer, 2014), p. 251

16 Abergel, D.S.L., Apalkov, V., Berashevich, J., *et al.*: 'Properties of graphene: a theoretical perspective', *Adv. Phys.*, 2010, **59**, (4), pp. 261–482

17 Chakraborty, T., Apalkov, V.: 'Aspects of the fractional quantum Hall effect in graphene', in Aloki, H., Dresselhaus, M.S. (Eds): 'Physics of Graphene' (Springer, 2014), Ch. 8, pp. 251–300

18 Chakraborty, T., Apalkov, V.M.: 'Traits and characteristics of interacting Dirac fermions in monolayer and bilayer graphene', *Solid State Commun.*, 2013, **175**, pp. 123–131

19 Xu, M., Liang, T., Shi, M., *et al.*: 'Graphene-like two-dimensional materials', *Chem. Rev.*, 2013, **113**, (5), pp. 3766–3798

20 Dean, C.R., Wang, L., Maher, P., *et al.*: 'Hofstadter's butterfly and the fractal quantum Hall effect in Moiré superlattices', *Nature*, 2013, **497**, (7451), pp. 598–602

21 Hunt, B., Sanchez-Yamagishi, J.D., Young, A.F., *et al.*: 'Massive Dirac fermions and Hofstadter butterfly in a Van der Waals heterostructure', *Science*, 2013, **340**, (6139), pp. 1427–1430

22 Pomomarenko, L.A., Gorbachev, R.V., Yu, G.L., *et al.*: 'Cloning of Dirac fermions in graphene superlattices', *Nature*, 2013, **497**, (7451), pp. 594–597

23 Dean, C.R., Young, A.F., Meric, I., *et al.*: 'Boron nitride substrates for high-quality graphene electronics', *Nature nanotechnology*, 2010, **5**, (10), pp. 722–726

24 Decker, R., Wang, Y., Brar, V.W., *et al.*: 'Local electronic properties of graphene on a BN substrate via scanning tunneling microscopy', *Nano Lett.*, 2011, **11**, (6), pp. 2291–2295

25 Xue, J., Sanchez-Yamagishi, J., Bulmash, D., *et al.*: 'Scanning tunnelling microscopy and spectroscopy of ultra-flat graphene on hexagonal boron nitride', *Nat. Mater.*, 2011, **10**, (4), pp. 282–285

26 Rhim, J.-W., Park, K.: 'Self-similar occurrence of massless Dirac particles in graphene under a magnetic field', *Phys. Rev. B*, 2012, **86**, (23), p. 235411

27 Nemec, N., Cuniberti, G.: 'Hofstadter butterflies of bilayer graphene', *Phys. Rev. B*, 2007, **75**, (20), p. 201404(R)

28 Gat, O., Avron, J.E.: 'Magnetic fingerprints of fractal spectra and the duality of Hofstadter models', *New J. Phys.*, 2003, **5**, (1), pp. 44.1–44.8

29 Janecek, S., Aichinger, M., Hernandez, E.R.: 'Two-dimensional Bloch electrons in perpendicular magnetic fields: an exact calculation of the Hofstadter butterfly spectrum', *Phys. Rev. B*, 2013, **87**, (23), p. 235429

30 Latil, S., Henrard, L.: 'Charge carriers in few-layer graphene films', *Phys. Rev. Lett.*, 2006, **97**, (3), p. 036803

31 Lopes dos Santos, J.M.B., Peres, N.M.R., Castro Neto, A.H.: 'Graphene bilayer with a twist: electronic structure', *Phys. Rev. Lett.*, 2007, **99**, (25), p. 256802

32 Apalkov, V.M., Chakraborty, T.: 'Optical transitions at commensurate angles in a misoriented bilayer graphene in an external magnetic field', *Phys. Rev. B*, **84**, (3), p. 033408

33 Hass, J., Varchon, F., Millán-Otoya, J.E., *et al.*: 'Why multilayer graphene on 4H-SiC (000$\bar{1}$) behaves like a single sheet of graphene', *Phys. Rev. Lett.*, 2008, **100**, (12), p. 125504

34 Shallcross, S., Sharma, S., Pankratov, O.A.: 'Quantum interference at the twist boundary in graphene', *Phys. Rev. Lett.*, 2008, **101**, (5), p. 056803

35 Li, G., Luican, A., Lopes dos Santos, J.M.B., *et al.*: 'Observation of Van Hove singularities in twisted graphene layers', *Nat. Phys.*, 2010, **6**, (2), pp. 109–113

36 Mele, E.J.: 'Commensuration and interlayer coherence in twisted bilayer graphene', *Phys. Rev. B*, 2010, **81**, (16), p. 161405(R)

37 Bistritzer, R., MacDonald, A.H.: 'Transport between twisted graphene layers', *Phys. Rev. B*, 2010, **81**, (24), p. 245412

38 Bistritzer, R., MacDonald, A.H.: 'Moiré butterflies in twisted bilayer graphene', *Phys. Rev. B*, 2011, **84**, (3), p. 035440

39 Luican, A., Li, G., Reina, A., *et al.*: 'Single-layer behavior and its breakdown in twisted graphene layers', *Phys. Rev. Lett.*, 2011, **106**, (12), p. 126802

40 Kindermann, M., Uchoa, B., Miller, D.L.: 'Zero-energy modes and gate-tunable gap in graphene on hexagonal boron nitride', *Phys. Rev. B*, 2012, **86**, (11), p. 115415

41 Wallbank, J.R., Patel, A.A., Mucha-Kruczynski, M., *et al.*: 'Generic miniband structure of graphene on a hexagonal substrate', *Phys. Rev. B*, 2013, **87**, (24), p. 245408

42 Chen, X., Wallbank, J.R., Patel, A.A., *et al.*: 'Dirac edges of fractal magnetic minibands in graphene with hexagonal Moiré superlattices', *Phys. Rev. B*, 2014, **89**, (7), p. 075401

43 McCann, E., Falko, V.: 'Landau-level degeneracy and quantum Hall effect in a graphite bilayer', *Phys. Rev. Lett.*, 2006, **96**, (8), p. 086805

44 McCann, E.: 'Asymmetry gap in the electronic band structure of bilayer graphene', *Phys. Rev. B*, 2006, **74**, (16), p. 161403

45 Milton Pereira, J., Peeters, F.M., Vasilopoulos, P.: 'Landau levels and oscillator strength in a biased bilayer of graphene', *Phys. Rev. B*, 2007, **76**, (11), p. 115419

46 Gudmundsson, V., Gerhardts, R.R.: 'Effects of screening on the Hofstadter butterfly', *Phys. Rev. B*, 1995, **52**, (23), pp. 16744–16752

47 Gudmundsson, V., Gerhardts, R.R.: 'The Hofstadter energy spectrum for an interacting 2DEG', *Surf. Sci.*, 1996, **361–362**, pp. 505–508

48 'Manifestation of the Hofstadter butterfly in far-infrared absorption', *Phys. Rev. B*, 1996, **54**, (8), pp. R5223–R5226(R)

49 Pfannkuche, D., MacDonald, A.H.: 'Quantum Hall effect of interacting electrons in a periodic potential', *Phys. Rev. B*, 1997, **56**, (12), pp. R7100–R7103(R)

50 Doh, H., Salk, S.H.: 'Effects of electron correlations on the Hofstadter spectrum', *Phys. Rev. B*, 1998, **57**, (3), pp. 1312–1315

51 Apalkov, V.M., Chakraborty, T.: 'Gap structure of the Hofstadter system of interacting Dirac fermions in graphene', *Phys. Rev. Lett.*, 2014, **112**, (17), p. 176401

52 Chakraborty, T., Pietiläinen, P.: 'The quantum Hall effects' (Springer, 1995)

53 Chakraborty, T., Pietiläinen, P.: 'The fractional quantum Hall effect' (Springer, 1988)

54 Laughlin, R.B.: 'Anomalous quantum Hall effect: an incompressible quantum fluid with fractionally charged excitations', *Phys. Rev. Lett.*, 1983, **50**, (18), pp. 1395–1398

55 Laughlin, R.B.: 'Nobel lecture: fractional quantization', *Rev. Mod. Phys.*, 1999, **71**, (4), pp. 863–874

56 Apalkov, V.M., Chakraborty, T.: 'Fractional quantum Hall states of Dirac electrons in graphene', *Phys. Rev. Lett.*, 2006, **97**, (12), p. 126801

57 Apalkov, V.M., Chakraborty, T.: 'Controllable driven phase transitions in fractional quantum Hall states in bilayer graphene', *Phys. Rev. Lett.*, 2010, **105**, (3), p. 036801

58 Apalkov, V.M., Chakraborty, T.: 'Stable Pfaffian state in bilayer graphene', *Phys. Rev. Lett.*, 2011, **107**, (18), p. 186803

59 Apalkov, V.M., Chakraborty, T.: 'Incompressible states of Dirac fermions in graphene with anisotropic interactions', *Solid State Commun.*, 2014, **177**, (128)

60 Abergel, D.S.L., Chakraborty, T.: 'Long-range Coulomb interaction in bilayer graphene', *Phys. Rev. Lett.*, 2009, **102**, (5), p. 056807

61 Abergel, D.S.L., Apalkov, V.M., Chakraborty, T.: 'Interplay between valley polarization and electron–electron interaction in a graphene ring', *Phys. Rev. B*, 2008, **78**, (19), p. 193405

62 Abergel, D.S.L., Pietiläinen, P., Chakraborty, T.: 'Electronic compressibility of graphene: the case of vanishing electron correlations and the role of chirality', *Phys. Rev. B*, 2009, **80**, (8), p. 081408

63 Apalkov, V.M., Chakraborty, T.: 'Electrically tunable charge and spin transitions in Landau levels of interacting Dirac fermions in trilayer graphene', *Phys. Rev. B*, 2012, **86**, (3), p. 035401

64 Du, X., Skachko, I., Duerr, F., *et al.*: 'Fractional quantum Hall effect and insulating phase of Dirac electrons in graphene', *Nature*, 2009, **462**, (7270), pp. 192–195

65 Abanin, D.A., Skachko, I., Du, X., *et al.*: 'Fractional quantum Hall effect in suspended graphene: transport coefficients and electron interaction strength', *Phys. Rev. B*, 2010, **81**, (11), p. 115410

66 Bolotin, K.I., Ghahari, F., Shulman, M.D., *et al.*: 'Observation of the fractional quantum Hall effect in graphene', *Nature*, 2009, **462**, (7270), pp. 196–199

67 Ghahari, F., Zhao, Y., Cadden-Zimansky, P., *et al.*: 'Measurement of the $\nu = 1/3$ fractional quantum Hall energy gap in suspended graphene', *Phys. Rev. Lett.*, 2011, **106**, (4), p. 046801

68 Yu, G.L., Gorbachev, R.V., Tu, J.S., *et al.*: 'Hierarchy of Hofstadter states and replica quantum Hall ferromagnetism in graphene superlattices', *Nat. Phys.*, 2014, **10**, (7), pp. 525–529

69 von Klitzing, K., Chakraborty, T.: 'Taking stock of the quantum Hall effects: thirty years on', *Phys. Canada*, 2011, **67**, (3), pp. 161–164

70 Ghazaryan, A., Chakraborty, T., Pietiläinen, P.: 'Fractional quantum Hall effect in Hofstadter butterflies of Dirac fermions', arXiv preprint, 2014, arXiv:1408.3424

71 Zak, J.: 'Magnetic translation group', *Phys. Rev.*, 1964, **134**, (6A), pp. A1602–A1606

72 Brown, E.: 'Bloch electrons in a uniform magnetic field', *Phys. Rev.*, 1964, **133**, (4A), pp. A1038–A1044

73 Haldane, F.D.M.: 'Many-particle translational symmetries of two-dimensional electrons at rational Landau-level filling', *Phys. Rev. Lett.*, 1985, **55**, (20), pp. 2095–2098

74 Kol, A., Read, N.: 'Fractional quantum Hall effect in a periodic potential', *Phys. Rev. B*, 1993, **48**, (12), pp. 8890–8898

75 The periodic rectangular geometry was extensively used earlier in the study of the FQHE in various situations. For example, see Chakraborty, T.: 'Spin-reversed ground state and energy gap in the fractional quantum Hall effect', *Surf. Sci.*, 1990, **229**, (1–3), pp. 16–20, and also Refs. [76–82]

76 Chakraborty, T.: 'Electron spin transitions in quantum Hall systems', *Adv. Phys.*, 2000, **49**, (8), pp. 959–1014

77 Chakraborty, T., Pietiläinen, P.: 'Thermodynamics and spin polarizations of the fractional quantum Hall states', *Phys. Rev. Lett.*, 1996, **76**, (21), pp. 4018–4021

78 Chakraborty, T., Pietiläinen, P.: 'Fractional quantum Hall effect in tilted magnetic fields', *Phys. Rev. B*, 1989, **39**, (11), pp. 7971–7973

79 Apalkov, V.M., Chakraborty, T., Pietiläinen, P., *et al.*: 'Half-polarized quantum Hall states', *Phys. Rev. Lett.*, 2001, **86**, (7), pp. 1311–1314

80 Chakraborty, T., Pietiläinen, P., Zhang, F.C.: 'Elementary excitations in the fractional quantum Hall effect and the spin-reversed quasiparticles', *Phys. Rev. Lett.*, 1986, **57**, (1), pp. 130–133

81 Chakraborty, T., Zhang, F.C.: 'Role of reversed spins in the correlated ground state for the fractional quantum Hall effect', *Phys. Rev. B*, 1984, **29**, (12), pp. 7032–7033(R)

82 Zhang, F.C., Chakraborty, T.: 'Ground state of two-dimensional electrons and the reversed spins in the fractional quantum Hall effect', *Phys. Rev. B*, 1984, **30**, (12), pp. 7320–7322(R)